Journal of Advances in Modeling Earth Systems

RESEARCH ARTICLE
10.1029/2018MS001406

On the Interplay Between Convective Aggregation, Surface Temperature Gradients, and Climate Sensitivity

David Coppin[1,2] and Sandrine Bony[1]

[1]Sorbonne Université, CNRS, LMD/IPSL, Paris, France, [2]Department of Physics, University of Auckland, Auckland, New Zealand

Key Points:
- Convective aggregation interacts strongly with surface temperature gradients
- Aggregation can increase climate sensitivity when coupled with an interactive slab ocean, rather than decreasing it
- The impact of convective aggregation on climate should also be investigated in coupled frameworks

Supporting Information:
- Supporting Information S1

Correspondence to:
D. Coppin,
d.coppin@auckland.ac.nz

Citation:
Coppin, D., & Bony, S. (2018). On the interplay between convective aggregation, surface temperature gradients, and climate sensitivity. *Journal of Advances in Modeling Earth Systems*, *10*. https://doi.org/10.1029/2018MS001406

Received 10 JUN 2018
Accepted 22 NOV 2018
Accepted article online 28 NOV 2018

Abstract This study explores the extent to which convective aggregation interacts with sea surface temperature (SST) and affects climate sensitivity. For this purpose, radiative-convective equilibrium simulations are run with a general circulation model coupled to an ocean mixed layer, and several types of perturbations are imposed to the ocean-atmosphere system. Convective aggregation turns out to be much more sensitive to temperature in coupled experiments than in prescribed SST experiments. But changes in convective aggregation induced by a doubling of the CO_2 concentration are always smaller than changes associated with the transition from a non-aggregated to an aggregated state. If aggregation changes were acting alone, they would exert a strong negative feedback on global mean surface temperature. However, in a coupled framework, aggregation changes interact with the SST and generate SST gradients that strengthen the positive low-cloud feedback associated with changes in SST pattern. This overcompensates the negative feedback due to aggregation changes and leads to a larger equilibrium climate sensitivity than in the absence of SST gradients. Although this effect might be model specific, interactions between convective aggregation and the spatial distribution of SST appear crucial to assess the impact of convective aggregation on climate sensitivity.

1. Introduction

An important metric for climate change studies is the equilibrium change in global mean near-surface air temperature that would result from a sustained doubling of the atmospheric carbon dioxide concentration, a quantity referred to as the equilibrium climate sensitivity (ECS). Although a precise estimate of the ECS has remained elusive for almost four decades (Charney et al., 1979; Stevens et al., 2016), much progress has been made in understanding the different physical processes that control it. In particular, recent studies have pointed out two factors that could modulate the strength of the water vapor and cloud feedbacks and therefore affect ECS. One of them is the role of convective organization (Holloway et al., 2017; Wing et al., 2017). As first hypothesized by Khairoutdinov and Emanuel (2010) with a toy model, the ability of deep convection to aggregate into clusters and to extend the area covered by clear, dry regions, would enhance the ability of the Earth to radiate heat to space and would lower ECS (Hohenegger & Stevens, 2016; Pierrehumbert, 1995). Recently, Cronin and Wing (2017) confirmed that this effect exists in cloud-resolving model channel radiative-convective equilibrium (RCE) simulations. Whether this mechanism also affects ECS in general circulation models (GCMs) remains an open issue (Mauritsen & Stevens, 2015).

Another factor that can influence ECS but remains poorly understood is the evolution of spatial patterns of sea surface temperature (SST) with global warming (Senior & Mitchell, 2000), an effect now referred to as "pattern effect" (Stevens et al., 2016). Depending on where and when a change in surface temperature takes place, it can exert a different radiative impact and strongly amplify or dampen the radiative feedbacks. This pattern effect, which is present in many models, has been shown to strongly influence cloud feedbacks and to induce an apparent time dependence of climate feedbacks (Andrews et al., 2012; Armour et al., 2013; Block & Mauritsen, 2013; Zhou et al., 2016). In particular, it is thought to be partly responsible for the apparent discrepancy between the ECS estimates inferred from historical climate records and the estimates derived from long-term climate change experiments from GCMs (Armour et al., 2013; Gregory & Andrews, 2016). Studies exploring the role of convective aggregation in climate sensitivity using the RCE framework often use prescribed and spatially uniform SST (Cronin & Wing, 2017). The question thus arises as to whether, and how, the impact of convective aggregation on climate sensitivity might depend on SST patterns. The question arises

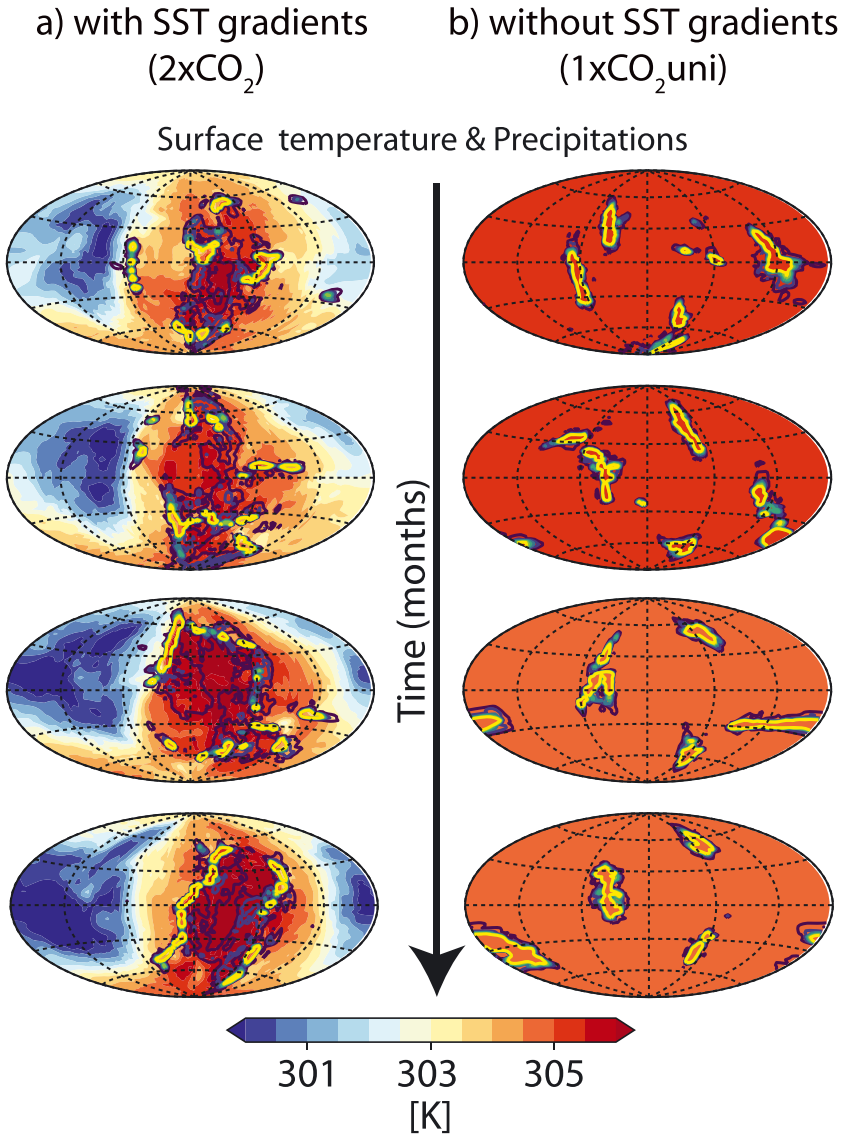

Figure 1. (a) Snapshots of surface temperature (color) and precipitation (contours from 5 to 30 mm/day) for different time steps separated by 1 month for simulation 2xCO_2. (b) Same as (a) but for simulation 1xCO_2uni. SST = sea surface temperature.

all the more that Coppin and Bony (2017) showed that convective aggregation and SST patterns can actually be closely coupled.

The aim of this paper is to use a GCM to explore how the interaction between SST gradients and convective aggregation modulates climate feedbacks and impacts the climate sensitivity in the idealized framework of RCE. We describe the experimental setup and the different experiments (section 2), look at the behavior of the simulation with SST gradients in 1CO_2 conditions and after an abrupt doubling of CO_2 (section 3 and 4), before discussing in more details the role of SST gradients on convective aggregation and climate sensitivity (section 5).

2. Model and Methods

We use the LMDZ5A GCM (Hourdin et al., 2006), the atmospheric component of the IPSL-CM5A-LR coupled ocean-atmosphere model, in the same non-rotating RCE configuration as in Coppin and Bony (2015, 2017). The RCE framework, which is widely used to understand the basic properties of the tropical atmosphere,

Table 1
Details of the Experiments Used in the Study

Simulation	Description
reference	Slab ocean simulation (10 m) forced by a CO_2 concentration of 285 ppm and initialized itself from a previous simulation run with a 20-m slab.
$1xCO_2$	Slab ocean simulation (10 m) starting from reference simulation whose humidity, temperature, SST, zonal, and meridional winds are globally averaged at the beginning. A white noise is added to the wind at the first atmospheric level to break symmetry. SST evolves freely. Different white noises on the wind field allow us to generate an ensemble of four simulations.
$1xCO_2$uni	Same as $1xCO_2$ but with the slab ocean temperature T_S spatially averaged at each time step to maintain the SST uniform. An ensemble of four simulations is formed with different white noise on the wind field.
$2xCO_2$	Slab ocean simulation (10 m) starting from the end of $1xCO_2$. Doubled CO_2 concentration. Different snapshots (same mean temperature and aggregation index as the mean in $1xCO_2$) are used to create an ensemble of four simulations.
$2xCO_2$uni	Slab ocean simulation (10 m) starting from the end of $1xCO_2$uni. Doubled CO_2 concentration. Slab ocean temperature spatially averaged at each time step. As for $2xCO_2$, different snapshots of $1xCO_2$uni (same mean temperature and aggregation index as the mean in $1xCO_2$uni) are used to create an ensemble of four simulations.
301 K	Prescribed and uniform SST simulations with a SST of 301 K and either a CO_2 concentration of 285 ppm (as in ; Coppin & Bony, 2015) or 570 ppm.
302 K	Same as 301 K with a SST of 302 K.
303 K	Same as 301 K with a SST of 303 K.
304 K	Same as 301 K with a SST of 304 K.
305 K	Same as 301 K with a SST of 305 K.

Note. SST = sea surface temperature.

corresponds to the statistical equilibrium state that the atmosphere and surface would reach in the absence of lateral energy transport (Emanuel et al., 2014).

The model has a horizontal resolution of 3.75° × 1.875° in longitude-latitude and 39 levels in the vertical (15 in the stratosphere). Its physical package (Hourdin et al., 2013) includes the Emanuel convection scheme (Emanuel, 1993), a statistical cloud scheme coupled to the convection scheme (Bony & Emanuel, 2001), a radiative transfer code (Morcrette, 1991), and a parameterization of the boundary layer as a diffusion with an eddy diffusivity, which depends on the local Richardson number and handles dry convection in the case of unstable profiles (Deardorff, 1972). For a detailed review of the LMDZ5A-LR GCM, see Hourdin et al. (2006) and Dufresne et al. (2013), and references therein.

The aquaplanet configuration of the model is used without rotation and employs a latitudinal discretization on a sinusoidal grid to ensure that the grid mesh area is uniform over the globe. It is forced by a constant and uniform insolation (1,066.78 W/m^2 with a zenith angle corresponding to 0° latitude and a diurnal cycle). The stratospheric ozone distribution is invariant and globally uniform (set to its mean equatorial profile). The ocean albedo is set to 0.07. Aerosol effects are not considered.

When coupled to a slab ocean mixed layer of 10-m depth, the model simulates a non-stationary RCE equilibrium (Coppin & Bony, 2017). This equilibrium remains roughly similar for a wide range of slab depths. Therefore, we choose a mixed layer depth of 10 m, as it allows us to simulate a global mean state representative of a large range of depths (up to 100 m) but reaches the equilibrium faster.

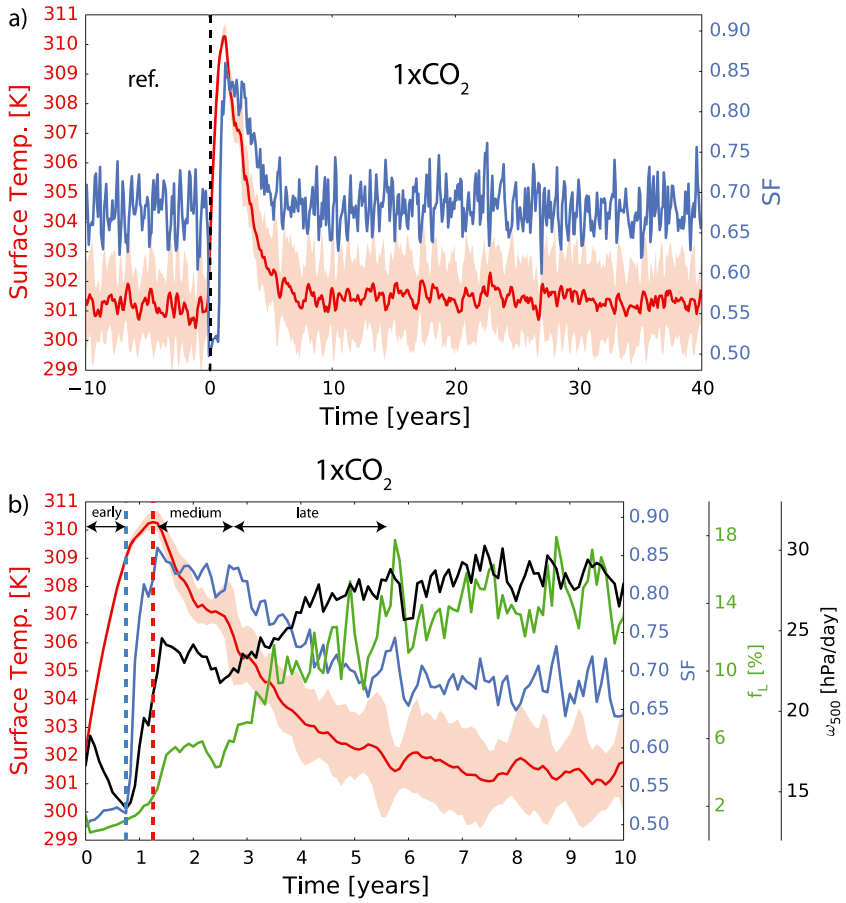

Figure 2. (a) Time evolution of surface temperature (red) and aggregation (SF, in blue) for the reference simulation and in 1xCO_2. The vertical black line indicates the time when the sea surface temperature, *q*, *T*, *u*, and *v* are spatially averaged. (b) Zoom over the first 10 years of 1xCO_2. The low-cloud fraction in the subsiding regions (green) and the vertical velocity at 500 hPa (black) in those regions are also reported. We call subsiding regions all model grid points where the vertical velocity at 500 hPa is positive. Shadings around the temperature line represent the 25th and 75th percentiles of the surface temperature. The vertical dashed blue and red lines indicate the start of self-aggregation and the beginning of the decrease in surface temperature, respectively. The periods noted as "early," "medium," and "late" are positioned over different periods to emphasize more easily the different transitions in Figures 3 and 4. SF = subsiding fraction.

To initialize slab simulations, we run a reference simulation forced by a CO_2 concentration of 285 ppm, initialized from a previous simulation run with a 20-m slab. The global mean surface equilibrium temperature of this reference simulation (called *ref*) is 301.2 K, and it exhibits significant SST gradients across the domain (SST ranging from 298 to 304 K) as well as an internal variability that significantly modulates the global mean temperature (Coppin & Bony, 2017). Note that in this paper, we will use the term gradient to refer to any spatial variability in SST, not in the sense of the spatial derivative of SST.

To assess the influence of SST gradients on convective aggregation and climate sensitivity under different forcings, we perform ensembles of four simulations, forced either by a 285 ppm or a 570 ppm concentration. The ensemble of 285 ppm experiments, called 1xCO_2, is initialized in each grid point by the globally averaged SST, temperature, humidity, and wind profiles from the reference simulation at equilibrium (end of year 50). Different members of a given ensemble differ only by the white noise applied on the wind at the beginning. The choice to start with uniform SST is motivated by two reasons. The first one is the wish to study self-aggregation in a coupled framework and to draw a parallel with prescribed and uniform SST experiments (Coppin & Bony, 2015). The second is that it allows us to study how the development of SST gradients interacts with convective aggregation. The ensemble of 2xCO_2 experiment is similar except that the CO_2 concentration is abruptly doubled at $t = 0$ (and then held constant) and it starts from the equilibrium state of the 1xCO_2 simulation. Different snapshots (same global mean temperature and aggregation index as in 1xCO_2 around equilibrium)

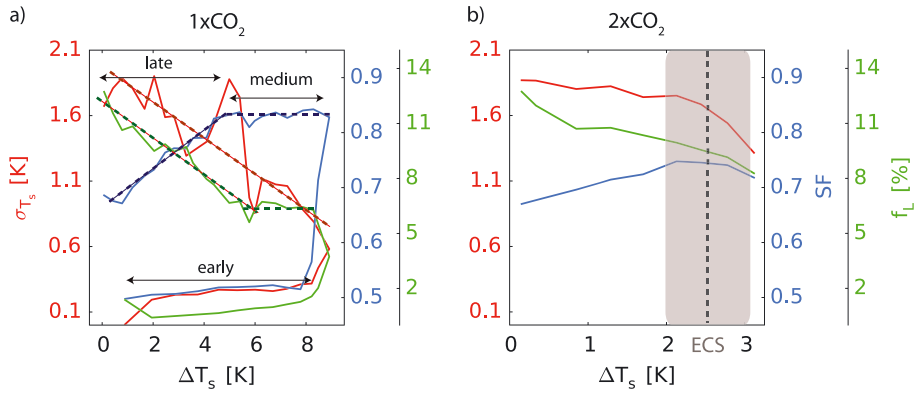

Figure 3. (a) Evolution of σ_{Ts} (red), convective aggregation SF (blue), and the low-cloud fraction in subsiding regions f_L (green) as a function of ΔT_S (difference between the surface temperature of the simulation and the equilibrium temperature of the reference simulation) in 1xCO$_2$. b) Same as (a) but in 2xCO$_2$. ΔT_S is calculated as the difference between the surface temperature of 2xCO$_2$ and the equilibrium temperature of 1xCO$_2$. σ_{Ts}, SF, and f_L are binned by sea surface temperature warming (bin size of 0.4 K, based on monthly averaged data). For 1xCO$_2$, the binning process is done separately for the periods before and after self-aggregation. The dashed lines in (a) are linear regressions designed to emphasize the transitions in low-cloud fraction and subsiding fraction. The vertical dashed gray line in (b) indicates the ECS of the 2xCO$_2$ simulation. The gray area around the ECS shows the range of temperature where the system is dominated by the internal variability around equilibrium and convective aggregation is out of phase with global mean surface temperature (cf. Coppin & Bony, 2017). The periods named early, medium, and late are the same as in Figure 2. SF = subsiding fraction; ECS = equilibrium climate sensitivity.

are used to create the ensemble of four simulations. In these simulations with gradients, convection is very mobile and moves toward the maximum SST (Figure 1a, cloud cover and surface wind in Figure S1a in the supporting information). At equilibrium, convective aggregation, SST gradients, and mean surface temperature are coupled via a feedback loop explained in details in Coppin and Bony (2017).

The impact of SST-atmosphere interactions is tested with ensembles of simulations 1xCO$_2$uni and 2xCO$_2$uni where the slab ocean temperature is spatially averaged at each time step (Figure 1b). In these simulations, convection organizes itself into three to five big clusters of convection, similar to what happens at high SST in prescribed, fixed and uniform SST simulations (Coppin & Bony, 2015). The realism of these two types of slab experiments is discussed in the supporting information (first section S1 and Figure S2) using less idealized configurations (Gates, 1992; Medeiros, et al., 2008). To discuss the similarities with the prescribed and uniform SST setup, we use the simulations from Coppin and Bony (2015) with SST ranging from 301 to 305 K and additional prescribed and uniform SST simulations over the same range of temperature with a doubled CO$_2$ concentration. All these experiments are listed in Table 1.

For clarity, only one simulation representative of each ensemble is presented in the paper. The main figures for each ensemble member are presented in the supporting information (section S2). Whenever a regression coefficient is mentioned in the paper, its value corresponds to the mean (and standard deviation) of this coefficient across the different members of each ensemble.

In this paper, self-aggregation solely refers to the transition from a non-aggregated state to an aggregated state, not to the convective aggregation changes between two aggregated states. The aggregation index used to quantify the degree of convective aggregation is the subsiding fraction (SF; Coppin & Bony, 2015). It corresponds to the fractional area of the domain covered by large-scale subsidence at 500 hPa, using daily outputs. This index characterizes the large-scale organization of convection, which is the only scale of organization represented in GCMs.

3. Interplay Between Aggregation and SST Gradients in 1CO$_2$ Climate

3.1. Impact of Self-Aggregation on Global Mean Surface Temperature

To study the impact of self-aggregation in 1CO$_2$ conditions, we start with disaggregated convection. Right after the homogenization at $t = 0$, the aggregation index SF is equal to 0.5 (Figures 2a and S3a). Because homogenizing the atmosphere induces a strong energetic disequilibrium, as long as convection remains disaggregated, the surface temperature increases rapidly. At some point, deep convection is triggered and rapidly self-aggregates (blue lines in Figures 2a, 2b, and S4a).

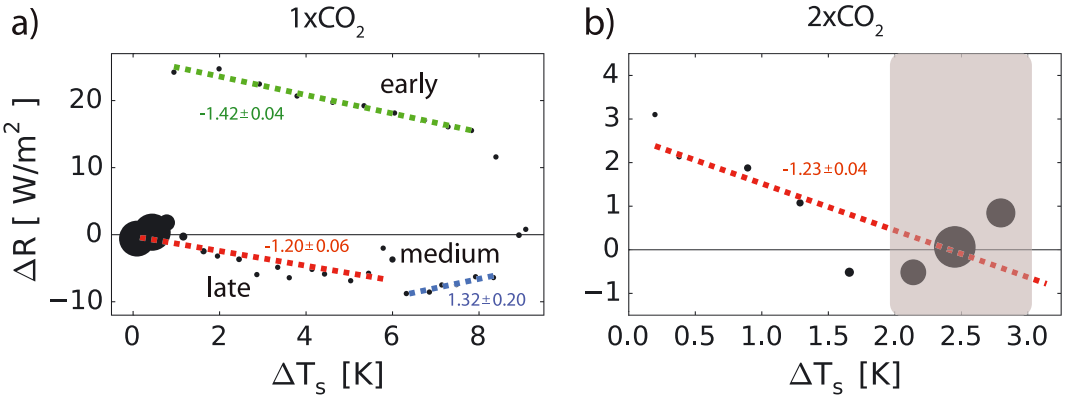

Figure 4. Evolution of ΔR as a function of ΔT_S for (a) $1xCO_2$ and (b) $2xCO_2$. ΔR is binned by sea surface temperature anomaly (using monthly data and bins of 0.4 K). For $1xCO_2$, ΔT_S and ΔR are calculated as differences with the equilibrium of the reference simulation. For $2xCO_2$, they are relative to the equilibrium of the $1xCO_2$ simulation. The size of the black circles indicates the number of points included in each bin. For $1xCO_2$, the binning process is done separately for the periods before and after self-aggregation. The colored dashed lines correspond to linear regression over different parts of $1xCO_2$ (early, medium, and late, respectively). Dashed lines of the same color have the same slope (see Table 2). The linear regression for $2xCO_2$ is calculated over the first 10 years to avoid the equilibrium period during which ΔR is dominated by internal variability (gray area). Identical color indicates the same value. All coefficient values and standard deviation ($W/m^2/K$) are calculated over the ensembles (Figures S6 and S7).

Before self-aggregation occurs (phase called "early"), the surface temperature rises uniformly and σ_{Ts}, the spatial standard deviation of SST over the globe (our proxy for SST gradients) remains very low (red line in Figures 3a and S3a). The radiative imbalance at the top of the atmosphere ΔR decreases slowly (green dashed line in Figures 4a and S6). As soon as self-aggregation is triggered (blue line going up in Figure 3a), ΔR exhibits a large drop that precedes a rapid decrease in global mean surface temperature, suggesting a strong cooling effect of self-aggregation. Indeed, as soon as aggregation is maximum, the global mean surface temperature drops (Figure 2b). This is consistent with the findings of Hohenegger and Stevens (2016) obtained using another GCM. As temperature decreases back to the equilibrium temperature of the reference simulation, SF also starts to decrease until it goes back to the reference temperature level, suggesting a role of convective aggregation in the regulation of temperature, at least under certain conditions.

3.2. Control of Global Mean Temperature and Aggregation by SST Gradients

As soon as deep convection is triggered, local SST gradients of small amplitude appear, mainly because of the shadowing effect of deep convective clouds on the underlying surface and the increased surface evaporation they generate in their surrounding. But it is only once these SST gradients of small amplitude have reached a sufficiently large scale and force convection to move toward the warm regions that convective self-aggregation is triggered (see section 5.1). The amplitude of the SST gradients is so small that, when stratified by the large-scale velocity at 500 hPa over the 300 days following the maximum of self-aggregation, the SST is almost uniform (darkest red line in Figure 5a). Then, the amplitude of SST gradients between convective and subsidence regimes increases almost linearly as the system cools down (red line in Figure 3a). Note that a minimum fraction of low-cloud fraction appears once convective aggregation generates a sufficiently strong subsidence in the subsiding regions (between 1.5 and 2.5 years in Figure 2b).

Inspection of $1xCO_2$ shows that the return to the equilibrium temperature of the reference simulation is made possible because of the increase in the low-cloud fraction that occurs after a sufficiently large cooling (around $\Delta T_S = +6$ K, green line in Figure 3a). At that time, the subsidence triggered by convective aggregation generates areas of strong static stability in the cold subsiding regions and promotes the formation of low clouds. Through their contribution to the planetary albedo, their shadowing effect on the underlying SST and their interaction with surface fluxes, the formation of these clouds enhances the cooling of the system and help temperature to go back to its equilibrium value.

To highlight the evolution of the SST contrast between convective and subsidence regions and its link to the low-cloud fraction as the global climate cools in $1xCO_2$ (from red to blue as time passes in Figures 5a and 5b), the low-cloud fraction is stratified by the large-scale vertical velocity at 500 hPa. The surface temperature first

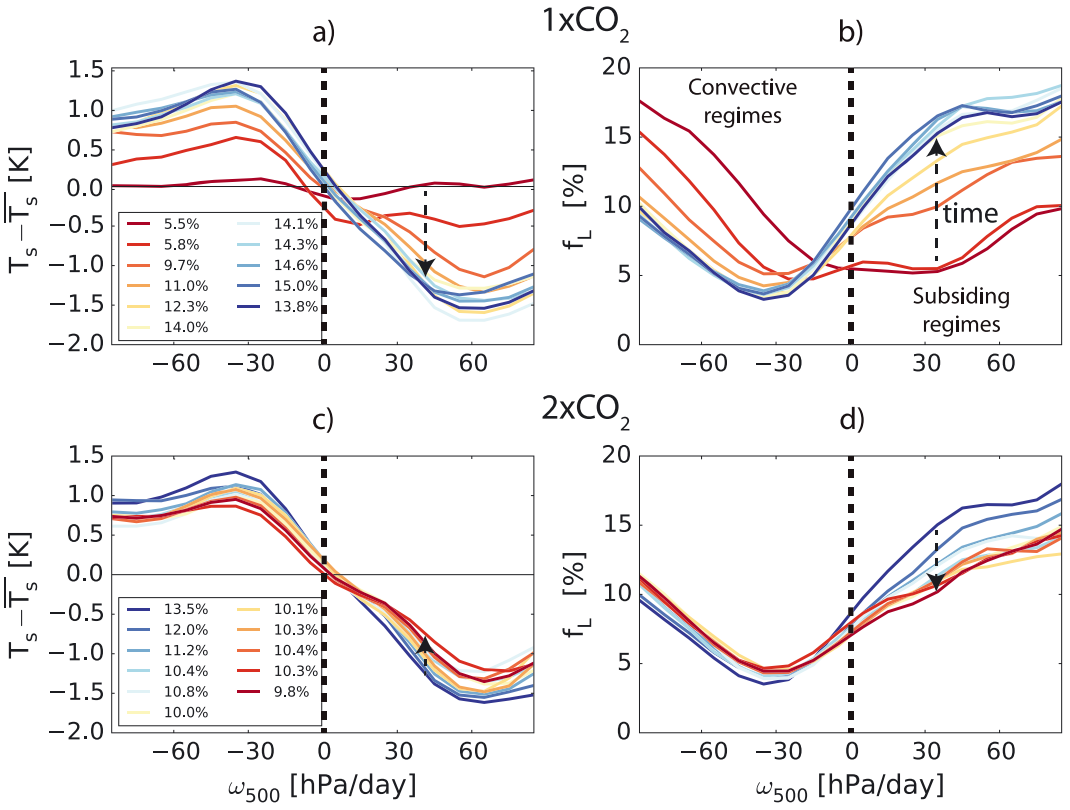

Figure 5. (a) Anomalies of surface temperature (relative to the globally averaged value) and (b) low-cloud amount stratified by the vertical velocity at 500 hPa for simulation 1xCO_2. (c) is the same as (a), and (d) is the same as (b) but for simulation 2xCO_2. Colors follow time in each simulation but are reversed between the two simulations so that global mean surface temperature always increases from blue to red. For the 1xCO_2 simulation, the first time step indicated by the red line corresponds to the period just after self-aggregation (beginning of "medium" period, after red dashed line in Figure 2b). The 2xCO_2 starts from the beginning with the dark blue line. The mean global fraction of low clouds in the subsidence regions is specified in the box. Each line is a time average over 300 consecutive days. Dashed black arrows indicate the time evolution.

decreases almost uniformly while only a small amount of low clouds (~6%) is present in the main subsiding regions (around 20–30 hPa/day in Figure 5b). The presence of low clouds helps to cool the subsidence regions and then to increase the SST gradient between subsidence and convection regions. This likely triggers the formation of additional low clouds in the cold subsiding regions, which further strengthens the SST gradients. When the gradients become strong enough, the subsidence is amplified and further reinforces the cooling by increasing the amount of low clouds.

To summarize, depending on the impact of low clouds on the surface, the system can experience two different types of cooling: either a uniform cooling or a patterned cooling with subsiding regions cooling more than convective regions. Both types are at play in 1xCO_2. When the system is forced to cool from very high global surface temperature (just after convective self-aggregation; Figure 6a), this cooling is initially almost uniform, until a small amount of low clouds can sufficiently cool the underlying surface and generate SST gradients. These newly formed gradients in turn favor the low-cloud formation in some of the coldest regions of the domain (Figure 6b). The formation of this small amount of low clouds is primarily due to the large-scale circulation that emerges right after the triggering of self-aggregation and that increases the static stability in subsiding regions. When low clouds develop further, they tend to cool the underlying surface and thus to increase the SST gradients, thereby reinforcing the large-scale circulation that promoted their formation (Figure 6c). This positive feedback leads to a stronger decrease of the temperature in the cold cloudy regions and decreases the global temperature until the system reaches equilibrium. This mechanism explains why the equilibrium temperature of the system is influenced by the changes in SST pattern.

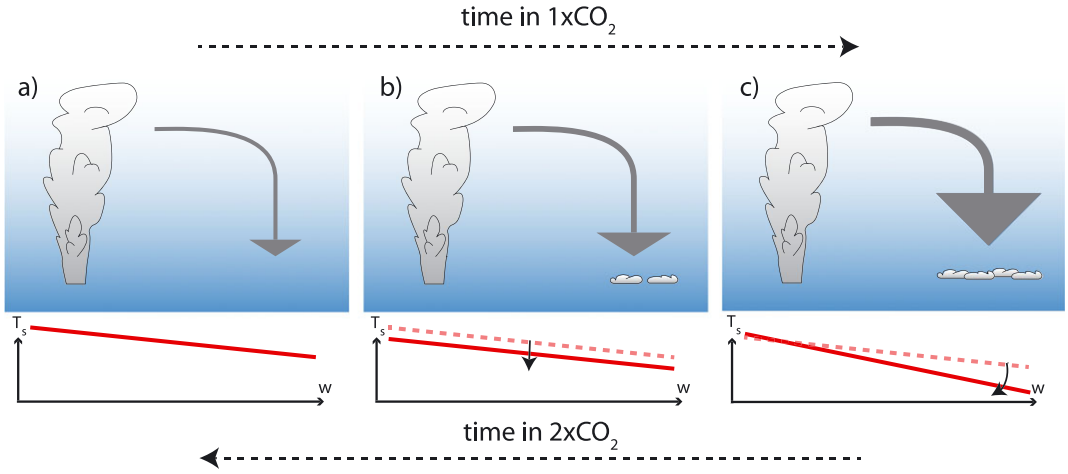

Figure 6. (a) Idealized large-scale subsidence (arrow) forced by the emergence of convective aggregation and a sea surface temperature (SST) gradient of small amplitude (red line), with convection above warm SSTs and clear-sky areas above cold SSTs. (b) Formation of boundary layer clouds over the cold, subsiding regions capped by a temperature inversion due to this large-scale circulation while the system cools uniformly until it reaches a temperature where low clouds can influence the surface significantly and strengthen the SST gradients. (c) The increased SST gradient reinforces the large-scale circulation and the low-cloud amount over the cold subsiding regions, which cools the subsiding regions further, hence strengthening the spatial gradient of SST between convective and subsiding regions, as well as the large-scale circulation.

3.3. Modulation of Climate Feedback by SST Gradients

The 1xCO_2 simulation gives us the opportunity to estimate the total feedback parameter λ. We estimate it using a Gregory-like approach (Gregory et al., 2004), that is, by calculating the slope of the linear regression between ΔR and ΔT_S (lines in Figure 4a). As long as self-aggregation is not triggered, the system is transitioning toward an equilibrium without convective aggregation: the radiative imbalance ΔR, which is maximum after the homogenization of the atmosphere decreases while temperature increases (early period, the slope of the green dashed line representing λ). After the triggering of self-aggregation, aggregation remains constant and strong for 2 years while the SST gradients increase and the system cools down (medium period). Once the low-cloud amount is large enough in the subsiding regions, convective aggregation decreases and λ changes ("late" period).

To isolate the relative influences of SST gradients and convective aggregation on the feedback parameter, we decompose it into three components. The first one does not depend on SST gradients nor aggregation. This "background" feedback, which includes other feedbacks such as the Planck response, water vapor, lapse-rate, and cloud feedbacks, corresponds to the green line with $\lambda = -1.42 \pm 0.02$ W/m^2/K in Figure 4a. The second component includes in addition the effect of SST gradients (blue line), and the third one includes the background feedback, the feedback from SST gradients, and the feedback associated with the interaction of convective aggregation with the SST gradients (red line).

To calculate the second component (background plus SST gradient feedback), we focus on the lower right branch of 1xCO_2 where convective aggregation and low clouds are constant but the SST gradients increase (between 6 and 8 K in Figure 3a). This medium period lasts only 2 years in the example shown and even less in the other members of the ensemble (Figures S4a and S5a). During this period, the net feedback parameter is positive and equal to $+1.32 \pm 0.20$ W/m^2/K (blue line in Figure 4a). Assuming that the background feedback remains similar implies that the positive feedback associated with the buildup of SST gradients is +2.74 W/m^2/K. This positive feedback may come from a reorganization of the circulation while aggregation remains constant.

To infer the feedback associated with convective aggregation (see Appendix A for an attempt to conceptualize the impact of aggregation on global mean surface temperature), we consider the red line in Figure 4a (part late). Assuming that the combined effect of the background plus the SST gradients remains similar, the negative feedback necessary to get the total climate feedback is the difference between the total feedback and this combined feedback (blue line), namely $-1.20-1.32 = -2.52$ W/m^2/K, the feedback due to aggregation

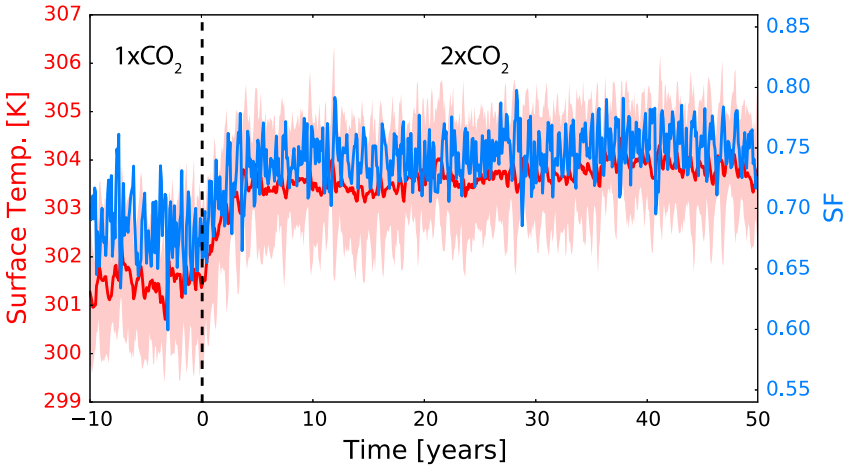

Figure 7. Time evolution of surface temperature (red) and aggregation (SF, in blue) for the end of $1xCO_2$ and $2xCO_2$. The vertical black line indicates the time when the CO_2 is abruptly doubled at the beginning of $2xCO_2$. Shadings around the temperature line indicate the 25th and 75th percentiles of the surface temperature. SF = subsiding fraction.

changes. Since this value also includes the low-cloud positive feedback that occurs when SST gets cooler, that is, below the 6 K warming in $1xCO_2$ (green line in Figure 3a), we expect the negative feedback of aggregation changes on temperature to be even stronger. However, in a coupled system with interactive SST gradients and preindustrial CO_2 conditions, its impact is more than compensated by the positive feedback associated with the change in SST pattern and low-cloud feedbacks (−2.52 vs. +2.74 W/m^2/K).

The question now arises whether this behavior is representative of a changing climate perturbed by an increase in greenhouse gases in the atmosphere. To answer this question, we analyze a $2xCO_2$ experiment.

4. Interplay Between Aggregation and SST Gradients in a Changing Climate

4.1. Relative Effects of Temperature and CO_2 on Convective Aggregation

When CO_2 is doubled, convective aggregation and global surface temperature increase together (Figures 7 and S3b). This behavior resembles what happens when the same model is forced by prescribed uniform SSTs (Coppin & Bony, 2015), although in the latter, convective aggregation saturates at high SSTs. In prescribed SST simulations, the change in convective aggregation resulted only from surface temperature changes. In doubled CO_2 experiments run in a coupled framework, it can result from temperature changes but also from a direct effect of CO_2, not mediated by surface temperature changes. To quantify these two contributions, we decompose the change in aggregation (SF) as follows:

$$\Delta SF = \left(\frac{\partial \mathrm{SF}}{\partial \mathrm{T_S}}\right)_{\mathrm{CO_2}} \times \Delta T_S + \left(\frac{\partial \mathrm{SF}}{\partial CO_2}\right)_{T_S} \times \Delta \mathrm{CO_2} \quad (1)$$

Estimates of $\left(\frac{\partial \mathrm{SF}}{\partial \mathrm{T_S}}\right)_{\mathrm{CO_2}}$ and $\left(\frac{\partial \mathrm{SF}}{\partial \mathrm{CO_2}}\right)_{\mathrm{T_S}}$ from our RCE experiments are given in Table 2.

For the prescribed SSTs experiments, we use the same range of temperature as displayed in the slab experiments (from 301 to 307 K) and additional simulations with doubled CO_2 and unchanged SSTs to investigate the direct effect of CO_2 on aggregation: $\left(\frac{\partial \mathrm{SF}}{\partial \mathrm{CO_2}}\right)_{T_S}$, $\left(\frac{\partial \mathrm{SF}}{\partial T_S}\right)_{\mathrm{CO_2}}$ and $\left(\frac{\partial R}{\partial T_S}\right)_{\mathrm{CO_2}}$ are calculated between SST and SST+2K experiments.

For coupled simulations, on the other hand, the first two coefficients are inferred from the linear regression between SF and the global mean surface temperature: $\left(\frac{\partial SF}{\partial T_S}\right)_{\mathrm{CO_2}}$ is the slope and $\left(\frac{\partial \mathrm{SF}}{\partial \mathrm{CO_2}}\right)_{T_S}$ the y intercept. $\left(\frac{\partial R}{\partial T_S}\right)_{\mathrm{CO_2}}$ is inferred from the linear regression between ΔR and ΔT_S in the simulation ensembles (Figures S6–S9).

Table 2 shows that the direct effect of CO_2 on aggregation is always positive. This may be a consequence of the stability-iris effect present in these simulations (Bony et al., 2016): the CO_2 forcing increases the static stability in the anvil cloud region, reducing the radiatively driven divergence and the anvil cloud fraction, which narrows the convective areas. This direct effect of CO_2 on aggregation is at least 3 times smaller in the

Table 2
Value of $\left(\frac{\partial SF}{\partial T_S}\right)_{CO_2}$, $\left(\frac{\partial SF}{\partial CO_2}\right)_{T_S}$, *and* $\left(\frac{\partial R}{\partial T_S}\right)_{CO_2}$ *Calculated for Prescribed and Uniform SST, and for Slab Experiments*

SST	Name	$\left(\frac{\partial SF}{\partial T_S}\right)_{CO_2}$ $\times 10^{-2}(1/K)$	$\left(\frac{\partial SF}{\partial CO_2}\right)_{T_S}$ $\times 10^{-1}$ $(1/[CO_2])$	$\left(\frac{\partial R}{\partial T_S}\right)_{CO_2}$ $= \lambda$ (W/m^2K)
Non-interactive SSTs	301 K	2.5	1.2	−5.0
	302 K	3.0	0.9	−2.3
	303K	2.0	0.7	−1.0
	304 K	0.4	0.3	−1.6
	305 K	1.1	0.4	−1.5
Interactive SSTs	$1xCO_2$ (301.2 K)	3.3	—	−1.42 ± 0.04 (green) +1.32 ± 0.20 (blue) −1.20 ± 0.06 (red)
	$2xCO_2$ (303.7 K)	3.5	0.1	−1.23 ± 0.04 (red)
	$1xCO_2$uni (305.2 K)	—	—	−1.41 ± 0.01 (top green) −1.45 ± 0.06 (bottom green)
	$2xCO_2$uni (307.2 K)	0.1	0.1	−1.42 ± 0.09 (green)

Note. The $1CO_2$ experiments are taken from Coppin and Bony (2015), and additional $2CO_2$ simulations are run to calculate $\left(\frac{\partial SF}{\partial CO_2}\right)_{T_S}$. $\left(\frac{\partial R}{\partial T_S}\right)_{CO_2}$ is calculated between SST and SST+2K (i.e., between 301 and 303 K for the line 301 K). For each slab simulation, the first two coefficients are inferred from the linear regression between SF and the global mean surface temperature. $\left(\frac{\partial R}{\partial T_S}\right)_{CO_2}$ is inferred from ΔR and ΔT_S in the different ensembles (Figures S6–S9). Color in brackets indicates the color of the regression line. Number between brackets under the name of each slab experiment is its equilibrium temperature. SF = subsiding fraction; SST = sea surface temperature

coupled experiments than in prescribed uniform SST experiments. On the contrary, convective aggregation is more sensitive to temperature in coupled simulations with interactive SST than in prescribed SST experiments, especially at high SSTs.

Therefore, in $2xCO_2$ simulation, which has an equilibrium surface temperature 2.5 K higher than in $1xCO_2$, 80% of the increase in aggregation is mediated by the surface temperature increase.

4.2. Limitation of Aggregation Changes by SST Gradients

A striking feature highlighted by Figure 7 is the relatively small change in aggregation after the doubling of CO_2. The difference between the two equilibrium states is of the same order as the internal variability of aggregation before the CO_2 doubling and much smaller than the change in aggregation associated with the transition from a non-aggregated to an aggregated state. In Figure 7, SF also remains much lower than its maximum value (0.85) observed in $1xCO_2$ after self-aggregation (Figure 2).

The comparison between Figures 4a and 4b shows that the total climate feedback of -1.23 ± 0.04 W/m^2/K for the $2xCO_2$ ensemble is equal to the total climate feedback of the $1xCO_2$ ensemble over the late period (Table 2 and red lines in Figure 4). This suggests similar feedbacks, although the system is experiencing a global warming in $2xCO_2$ and a global cooling in late $1xCO_2$. In both cases, the convection is already aggregated and undergoes a change in global mean temperature with freely evolving SST gradients. Consistently, the regime distributions of SST and low clouds are similar in $1xCO_2$ and $2xCO_2$, and the change in SST pattern present in $1xCO_2$ is also found in $2xCO_2$, even though with a smaller amplitude because the global SST change is much smaller (Figures 5c and 5d). This means that in $2xCO_2$, as the surface temperature increases, the low-cloud fraction and SST gradients decrease, amplifying the warming even more (Figures 6c to 6a).

Similarly to what happens as part of internal variability (Coppin & Bony, 2017), the interplay between convection, SST gradients, and surface temperature is what limits convective aggregation and controls the total climate feedback. When convection is concentrated above the highest SST, convective aggregation reaches a maximum. But rapidly, the SST below convection decreases, as well as the SST gradients that maintained

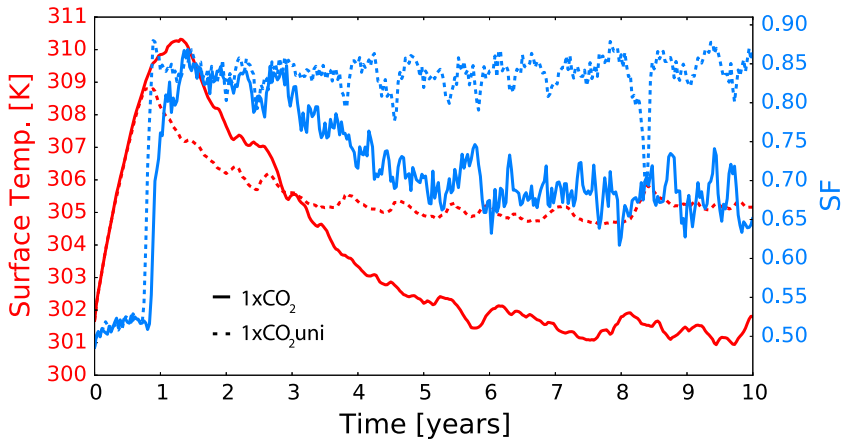

Figure 8. Same as Figure 2 but for 1xCO_2 (plain line) and 1xCO_2uni (dashed lines). SF = subsiding fraction.

the large-scale circulation necessary for convective aggregation. Therefore, convection disaggregates before reaggregating once the differential surface warming between convective and subsiding zones develops large-scale SST gradients again. As long as the surface temperature increases in response to the CO_2 forcing, convective aggregation gradually increases but the magnitude of the increase is limited by this mechanism. Once at equilibrium, this feedback loop generates some internal variability in global mean surface temperature (Coppin & Bony, 2017). This explains why aggregation, SST gradients, and low-cloud fraction decrease together around the equilibrium temperature, and why ΔR increases with temperature in 2xCO_2 above ΔT_S = 2 K in Figures 3b and 4b respectively.

These results suggest that the interaction between SST gradients and convective aggregation acts to limit the magnitude of the aggregation change and therefore the strength of the stabilization effect exerted by aggregation changes.

5. What Happens in the Absence of SST Gradients?

To further assess the effect of the SST gradients on convective aggregation, we analyze experiments called 1xCO_2uni and 2CO_2uni where the SST gradients are removed at each time step by spatially averaging the SST. The SST is thus interactive but remains spatially uniform within the domain.

5.1. Faster Self-Aggregation

The 1CO_2 ensembles of simulations run with or without SST gradients start from uniform conditions and without any large-scale circulation. As long as a large-scale circulation does not develop, the surface temperature remains nearly homogeneous, even when SST gradients are free to develop, and the two ensembles of simulations are almost identical (first months in Figure 8). They start to diverge as soon as deep convection and a large-scale circulation emerge, and promotes the development of SST gradients. In 1xCO_2uni, convective aggregation increases very quickly and reaches a maximum shortly after the start of the self-aggregation process. In contrast, in 1xCO_2, aggregation increases more slowly and therefore the system keeps warming for a longer time until aggregation reaches its maximum and temperature starts to decrease.

This different behavior between 1xCO_2 and 1xCO_2uni is directly related to the emergence of SST gradients in 1xCO_2once deep convection is triggered. The ocean below convective clouds cools down, mainly because of the shadowing effect of clouds on the surface and the increase in evaporation in the vicinity, thus favoring the emergence of SST gradients. The slight cooling of SST under convective clouds relative to non-convective areas generates a circulation that opposes the shallow circulation that gives rise to convective self-aggregation (Hohenegger & Stevens, 2016). It becomes harder for convection to self-aggregate, hence the delayed self-aggregation. It is only when SST gradients cover a sufficiently large area of the domain that convection moves toward the warmest SSTs and that the system starts to cool.

5.2. Impact on Climate Feedbacks

Even though the system in 1xCO_2uni stabilizes at a much higher global temperature than 1xCO_2 (warmer by 4 K, Figure 8), the initial cooling following self-aggregation is qualitatively similar to the uniform cooling that

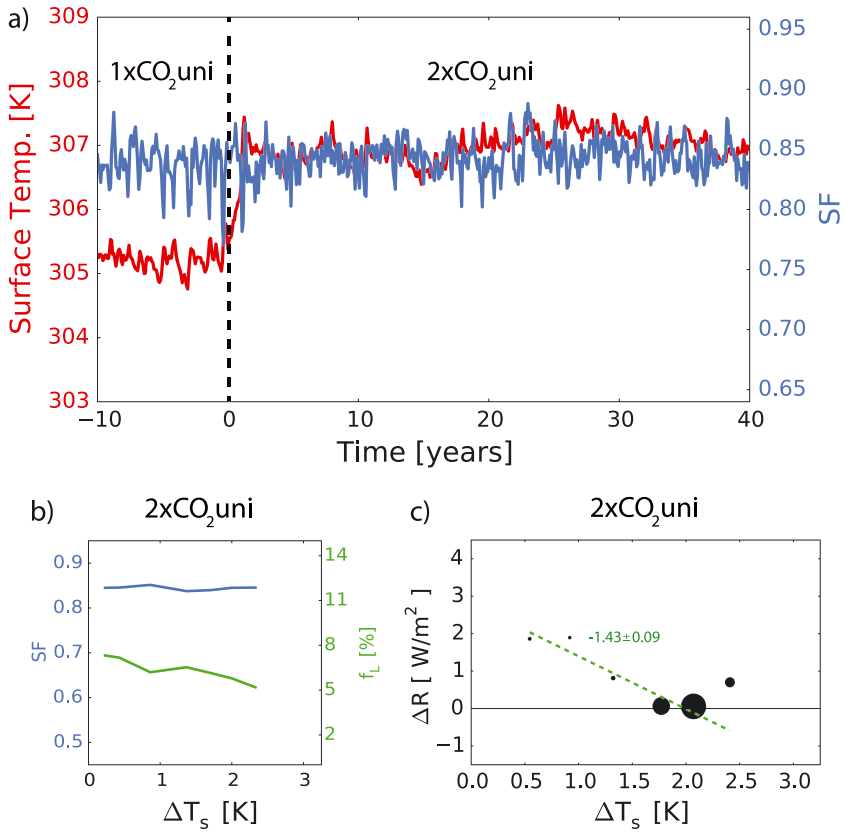

Figure 9. Time evolution of surface temperature (red) and aggregation (SF, in blue) for the end of 1xCO_2uni and 2xCO_2uni. The vertical black line indicates the time when the CO_2 is abruptly doubled at the beginning of 2xCO_2uni. (b) Evolution of convective aggregation SF (blue) and the low-cloud fraction in subsiding regions f_L (green) as a function of ΔT_S (difference between the surface temperature of the simulation and the equilibrium temperature of 1xCO_2uni) for the simulation 2xCO_2uni. (c) Same as Figure 4 but for 2xCO_2uni. ΔT_S is calculated as the difference between the surface temperature of 2xCO_2uni and the equilibrium temperature of 1xCO_2uni. SF, f_L, ΔR, and ΔT_S are binned by sea surface temperature warming (bin size of 0.4 K with monthly averaged data). The green dashed line corresponds to $\lambda = -1.43$ W/m^2/K. SF = subsiding fraction.

happens over the medium period in 1xCO_2, as shown by Figures 3a and S5a–S5c. Both ensembles diverge when the SST gradients become strong enough to increase the subsidence velocity and the low-cloud cover in 1xCO_2 (black and green lines in Figure S4) and activate the feedback loop that leads to a further cooling of the system. This emphasizes the importance of SST gradients for the regulation of the global mean surface temperature of the coupled ocean-atmosphere system.

When the CO_2 concentration is abruptly doubled from the equilibrium of 1xCO_2uni, the global surface temperature increases by 2 K while convection aggregation (SF) remains constant (Figure 9). This saturation of convective aggregation at a very high value, as well as the way it is organized, is reminiscent of what happens at high surface temperature with prescribed uniform SSTs. The calculation of $\left(\frac{\partial SF}{\partial T_S}\right)_{CO_2}$ and $\left(\frac{\partial SF}{\partial CO_2}\right)_{T_S}$ (0.1×10^{-2} K^{-1} and 0.1×10^{-1} [CO_2]$^{-1}$, respectively, Table 2) confirms that, in the absence of SST gradients, convective aggregation behaves like in experiments with prescribed uniform SSTs (section 4.1), thus confirming that simulations with SST gradients exhibit a weaker direct effect of CO_2 but a stronger sensitivity to temperature.

Convective aggregation does not increase further with temperature. Yet the climate feedback parameter $\lambda = -1.42$ W/m^2/K is more negative in 2xCO_2uni than in 2xCO_2, leading to a lower ECS (2 K compared to 2.5 K in 2xCO_2). The slope of the green dashed lines in Figures 9c and 4a (or Figures S8 and S9) suggests that it does not result from a dependence on the mean state. On the other hand, even if the low-cloud fraction is still decreasing in 2xCO_2uni (Figure 9b), its decrease rate is weaker than in 2xCO_2 (Figure 3b). Low clouds are less sensitive to the increase in surface temperature when SST gradients are absent. This results in a much smaller positive low-cloud feedback in the absence of SST gradients (no robust positive trend emerges) than with SST

gradients: 0.5 W/m^2/K in 2xCO_2 (not shown). The total climate feedback is thus more negative and the ECS lower in 2xCO_2uni compared to 2xCO_2.

These findings emphasize the fact that the coupling of the atmosphere with SST fundamentally affects the system's response to a global increase in surface temperature. The framework with uniform but evolving SST shares a lot of similarities with the prescribed and uniform high SST simulations: same organization of convection, saturation of convective aggregation for high SST, stronger dependence of aggregation on CO_2 rather than on surface temperature, and same large-scale circulation. On the contrary, the framework with interactive SST is more representative of less idealized setups (Figure S2). This study thus casts doubt on the ability of the prescribed SST framework to correctly assess the impact of convective aggregation on the climate sensitivity, at least for our model.

Yet a large literature has shown how relevant prescribed SST frameworks can be to interpret climate feedbacks in coupled frameworks (e.g; Brient & Bony, 2013; Ringer et al., 2014). One possible explanation for this apparent contradiction could be the saturation of convective aggregation at high SST in our model. The prescribed SST framework might still be relevant to assess the impact of convective aggregation on climate in other models where this saturation does not occur or even at smaller SSTs when convective aggregation is not saturated (for models where it will saturate at higher SST). As a matter of fact, in our model, the organization of convection at these smaller SSTs is more similar across configurations (see Figures 2.7 and 2.8 of Coppin, 2017, for the same comparison as in section S1 between the reference simulation, a prescribed and uniform SST of 298 K, the AMIP (Atmospheric Model Intercomparison Project) simulation over the tropical oceans and AquaControl over the tropics). To answer this contradiction, the impact of convective aggregation on climate should be investigated with other models in coupled frameworks.

6. Conclusions and Discussion

This study investigates how the interaction between SST gradients and convective aggregation impacts climate feedbacks and the climate sensitivity in the idealized framework of RCE. For this purpose, different types of perturbations are applied to the system: either the atmosphere is abruptly homogenized spatially to start with disaggregated convection (and then left free to develop heterogeneities and aggregation again), which results in a large positive imbalance of the top-of-atmosphere radiation budget (1xCO_2 experiments), or the CO_2 concentration of the atmosphere is abruptly doubled in the atmosphere (2xCO_2 experiments). In addition, to further assess the role of SST patterns in the behavior of the coupled system, additional experiments are run without SST patterns; this is done by spatially homogenizing the SST field at each time step (experiments 1xCO_2uni and 2xCO_2uni).

These experiments show that the triggering of convective self-aggregation results in a strong and abrupt drop in global mean surface temperature. This triggering is slowed down in the presence of SST gradients because of the competition between two circulations: one associated with the mass convergence in deep convective areas and divergence in subsiding areas, and a shallow circulation induced by SST gradients (with convergence over warmer areas and subsidence over colder areas). This competition stops and self-aggregation starts cooling the system only when the spatial scale of the SST gradient is large enough to force convective clouds to move toward the warmest SSTs. When imposing a CO_2 doubling to an atmosphere already organized, the climate warms and convective aggregation increases. However, the magnitude of the aggregation change is much weaker than in a situation of convective self-aggregation when convection transitions from a non-aggregated state to an aggregated state.

The comparison of the total climate feedback parameter in the different experiments suggests that the (strong) negative feedback associated with the enhanced convective aggregation is more than offset by the (strong) positive feedback associated with the change in SST patterns and its interaction with the low-cloud cover. It suggests that due to the coupling between SST, convective aggregation and low-cloud cover (Coppin & Bony, 2017), the role that changes in aggregation play in climate sensitivity may not be as strong as speculated based on prescribed uniform SST experiments.

One may wonder whether these conclusions are model dependent. Indeed, the IPSL-CM5A GCM is known to produce a strong positive low-cloud feedback (Vial et al., 2013) and therefore to predict a large decrease of the low-cloud cover as the climate warms. Moreover, in this model an increase of convective aggregation is generally associated with an increase of the low-cloud cover (Coppin & Bony, 2015, 2017). The impact of

convective aggregation on climate sensitivity is likely to depend on the relative response of low-level clouds and convective aggregation to surface warming. Whether the compensation between the aggregation feedback and other feedbacks (primarily those associated with SST patterns and low clouds) is robust and occurs in models that predict a very different low-cloud feedback remains to be investigated.

In any case, the present results suggest that numerical experiments with uniform surface temperatures might be misleading because the response of convective aggregation to global mean surface temperature is different with and without SST gradients. The relative sensitivity of aggregation to SST and CO_2 differs between the uniform SST and the SST gradient frameworks. Indeed, for a given surface temperature anomaly, we find that the change in aggregation is generally larger in a coupled ocean-atmosphere framework than in any experiments in which the SST is uniform, be it prescribed or evolving (Table 2). This is because in a coupled framework with SST gradients, the interplay between surface temperature gradients and convective aggregation prevents aggregation from reaching its maximum and thus from "saturating" as it does more easily in the absence of interactive SSTs (Coppin & Bony, 2015; Cronin & Wing, 2017). This means that, in simulations with ocean-atmosphere interactions, convection may never reach a high degree of aggregation. It also emphasizes the fact that the link between SST gradient and aggregation may be crucial to assess the behavior of convective aggregation in a changing climate. Nevertheless, the difference observed between uniform SST and interactive SST configurations in our model may also result from the saturation of convective aggregation at high SST in the uniform SST setups. Theses differences might not hold for lower SSTs or for other models where convective aggregation does not saturate at high SST.

SST gradients strongly modulate feedbacks in our coupled RCE framework. They limit the impact of convective aggregation and add a strong positive feedback that overcompensates the negative feedback of aggregation. The latter point echoes results from GCMs where changes in the spatial distribution of tropical SST generate a pattern effect, causing changes in radiative feedbacks that are not included in the global mean temperature response to a forcing and that usually occur on different time scales (Andrews et al., 2015; Zhou et al., 2016). It is noteworthy that, in these studies as in the present one, the modulation of the radiative feedback by the SST happens via a strong control on the low-cloud fraction in the subsiding regions and thus on the shortwave cloud feedback.

Extending the discussion over more ancient periods where the climate was much warmer and considering that the low-cloud fraction continues to decrease with temperature, we can imagine a transition where low clouds eventually disappear when the lowest SST becomes too warm and the SST gradients are reduced relative to today's climate. With these high SSTs and weak SST gradients, would the climate become more similar to the uniform but evolving SST experiment ($2xCO_2$uni) and its high degree of aggregation? In that state where aggregation mostly depend on CO_2, would λ become much stronger (lower ECS when CO_2 increases)? These are all speculations, but understanding how convective aggregation is controlled by SST gradients in much warmer climates might be helpful to understand past and future climates.

Even if convective aggregation is not critical for climate sensitivity because of the countereffect of SST gradients, changes in convective aggregation could influence other aspects of climate change. For instance, they may contribute to the narrowing of convergence zones in a warmer climate, as discussed by Bony et al. (2016). This hypothesis remains to be tested in a multimodel framework and in observations.

Appendix A: On the Effect of SST Gradients as a Climate Feedback

The antagonist effects of convective aggregation and SST patterns in the control of climate sensitivity might be conceptualized by adding a term to the equation proposed by Cronin and Wing (2017). In this case, the top-of-atmosphere radiation R is the sum of $N(T)$, the state without aggregation nor SST gradients, plus, due to the fact that convective aggregation modulates the water vapor and cloud distributions, a product of a degree of aggregation, $A(T)$, and a difference $B(T)$ in top-of-atmosphere flux between aggregated and non-aggregated states, plus a product of the strength of SST gradients, $G(T)$, and a difference $C(T)$ in top-of-atmosphere flux between spatially uniform and heterogeneous SST:

$$R = N(T) + A(T)B(T) + G(T)C(T). \tag{A1}$$

When each term is considered to depend only on temperature, the total climate feedback λ becomes

$$\lambda = \frac{dR}{dT} \tag{A2}$$

$$= \frac{dN}{dT} + A\frac{dB}{dT} + B\frac{dA}{dT} + G\frac{dC}{dT} + C\frac{dG}{dT}. \quad \text{(A3)}$$

The first term is the climate feedback without aggregation and SST gradient. The second and third terms correspond to the influence of convective aggregation on λ, while the fourth and fifth represent the influence of SST gradients. In our prescribed and uniform SST experiments and in Cronin and Wing (2017), $A\frac{dB}{dT}$, the effect of aggregation on the radiative budget (especially via humidity changes in dry regions and the fact that the difference in clear-sky outgoing longwave radiation between a moist and dry atmosphere increasingly diverges with warming), is the main contributor to the negative feedback of aggregation. But, due to the compensations between clear-sky and cloud feedbacks and maybe because convection is much more mobile with SST gradients (Coppin & Bony, 2017), it is largely offset, in coupled RCE experiments, by $B\frac{dA}{dT}$, the term associated with aggregation changes, and $C\frac{dG}{dT}$, related to changes in SST gradients. We expect $G\frac{dC}{dT}$, the change in top-of-atmosphere radiation budget with increasing SST when the SST gradients are constant, to be positive but smaller than $C\frac{dG}{dT}$, except when the SST gradients become minimum, that is, when low clouds have completely disappeared.

Acronyms

RCE = Radiative-convective equilibrium
SST = Sea surface temperature
CRM = Cloud-Resolving Model
GCM = General circulation model
SF = Subsiding fraction
f_L = Fraction of low clouds in subsiding regions
σ_{Ts} = Standard deviation of surface temperature, proxy for SST gradients

Acknowledgments
We thank Adrian Tompkins, Cathy Hohenegger, Caroline Muller, Jean-Pierre Chaboureau, and Jean-Yves Grandpeix for many useful discussions during the development of this work. We also thank Tim Cronin and an anonymous reviewer for their insightful comments. This work was granted access to the HPC resources of the Institut du développement et des ressources en informatique scientifique (IDRIS) under the allocation 0292 made by GENCI. We acknowledge support from UPMC (Université Pierre et Marie Curie) and the European Research Council (ERC) EUREC^{4}A grant 694768. All the data used in this study are available at ftp://ftp.lmd.jussieu.fr/pub/dcoppin/data_article_interplay_aggreg_sst/.

References

Andrews, T., Gregory, J. M., & Webb, M. J. (2015). The dependence of radiative forcing and feedback on evolving patterns of surface temperature change in climate models. *Journal of Climate*, *28*(4), 1630–1648. https://doi.org/10.1175/JCLI-D-14-00545.1

Andrews, T., Gregory, J. M., Webb, M. J., & Taylor, K. E. (2012). Forcing, feedbacks and climate sensitivity in CMIP5 coupled atmosphere-ocean climate models. *Geophysical Research Letters*, *39*, L09712. https://doi.org/10.1029/2012GL051607

Armour, K. C., Bitz, C. M., & Roe, G. H. (2013). Time-varying climate sensitivity from regional feedbacks. *Journal of Climate*, *26*(13), 4518–4534. https://doi.org/10.1175/JCLI-D-12-00544.1

Block, K., & Mauritsen, T. (2013). Forcing and feedback in the MPI-ESM-LR coupled model under abruptly quadrupled CO 2. *Journal of Advances in Modeling Earth Systems*, *5*, 676–691. https://doi.org/10.1002/jame.20041

Bony, S., & Emanuel, K. A. (2001). A Parameterization of the cloudiness associated with cumulus convection; Evaluation using TOGA COARE data. *Journal of the Atmospheric Sciences*, *58*(21), 3158–3183. https://doi.org/10.1175/1520-0469(2001)058<3158:APOTCA>2.0.CO;2

Bony, S., Stevens, B., Coppin, D., Becker, T., Reed, K. A., Voigt, A., & Medeiros, B. (2016). Thermodynamic control of anvil cloud amount. *Proceedings of the National Academy of Sciences*, *113*(32), 8927–8932.

Brient, F., & Bony, S. (2013). Interpretation of the positive low-cloud feedback predicted by a climate model under global warming. *Climate Dynamics*, *40*(9-10), 2415–2431. https://doi.org/10.1007/s00382-011-1279-7

Charney, J. G., Arakawa, A., Baker, D., Bolin, B., Dickinson, R. E., Goody, R. M., et al. (1979). Carbon dioxide and climate: A scientific assessment (National Academy of Sciences, 1979).

Coppin, D. (2017). Agrégation de la convection dans un modéle de circulation générale : mécanismes physiques et róle climatique (Ph.D. thesis), Université Pierre et Marie Curie, Paris VI. Retrieved from https://tel.archives-ouvertes.fr/tel-01596053/document

Coppin, D., & Bony, S. (2015). Physical mechanisms controlling the initiation of convective self-aggregation in a general circulation model. *Journal of Advances in Modeling Earth Systems*, *7*, 2020–2078. https://doi.org/10.1002/2015MS000571

Coppin, D., & Bony, S. (2017). Internal variability in a coupled general circulation model in radiative-convective equilibrium. *Geophysical Research Letters*, *44*, 5142–5149. https://doi.org/10.1002/2017GL073658

Cronin, T. W., & Wing, A. A. (2017). Clouds, circulation, and climate sensitivity in a radiative-convective equilibrium channel model. *Journal of Advances in Modeling Earth Systems*, *9*, 2833–2905. https://doi.org/10.1002/2017MS001111

Deardorff, J. W. (1972). Theoretical expression for the countergradient vertical heat flux. *Society*, *77*(30), 5900–5904.

Dufresne, J. L., Foujols, M. A., Denvil, S., Caubel, A., Marti, O., Aumont, O., et al. (2013). Climate change projections using the IPSL-CM5 Earth System Model: From CMIP3 to CMIP5. *Climate Dynamics*, *40*, 2123–2165. https://doi.org/10.1007/s00382-012-1636-1

Emanuel, K. A. (1993). The effect of convective response-time on WISHE modes. *Journal of Atmospheric Science*, *50*, 1763–1776. https://doi.org/10.1175/1520-0469(1993)050<1763:TEOCRT>2.0.CO;2

Emanuel, K. A., Wing, A. A., & Vincent, E. M. (2014). Radiative-convective instability. *Journal of Advances in Modeling Earth Systems*, *6*, 75–90. https://doi.org/10.1002/2013MS000270

Gates, W. L. (1992). AMIP: The Atmospheric Model Intercomparison Project. https://doi.org/10.1175/1520-0477(1992)073<1962:ATAMIP>2.0.CO;2

Gregory, J. M., & Andrews, T. (2016). Variation in climate sensitivity and feedback parameters during the historical period. *Geophysical Research Letters*, *43*, 3911–3920. https://doi.org/10.1002/2016GL068406

Gregory, J. M., Ingram, W. J., Palmer, M. A., Jones, G. S., Stott, P. A., Thorpe, R. B., et al. (2004). A new method for diagnosing radiative forcing and climate sensitivity. *Geophysical Research Letters*, *31*, L03205. https://doi.org/10.1029/2003GL018747

Hohenegger, C., & Stevens, B. (2016). Coupled radiative convective equilibrium simulations with explicit and parameterized convection. *Journal of Advances in Modeling Earth Systems*, *8*, 1468–1482. https://doi.org/10.1002/2013MS000282

Holloway, C. E., Wing, A. A., Bony, S., Muller, C., Masunaga, H., L'Ecuyer, T., et al. (2017). Observing convective aggregation. *Surveys in Geophysics*, *38*, 1199–1236. https://doi.org/10.1007/s10712-017-9419-1

Hourdin, F., Foujols, M. A., Codron, F., Guemas, V., Dufresne, J. L., Bony, S., et al. (2013). Impact of the LMDZ atmospheric grid configuration on the climate and sensitivity of the IPSL-CM5A coupled model. *Climate Dynamics*, *40*(9-10), 2167–2192. https://doi.org/10.1007/s00382-012-1411-3

Hourdin, F., Musat, I., Bony, S., Braconnot, P., Codron, F., Dufresne, J. L., et al. (2006). The LMDZ4 general circulation model: Climate performance and sensitivity to parametrized physics with emphasis on tropical convection. *Climate Dynamics*, *27*(7-8), 787–813. https://doi.org/10.1007/s00382-006-0158-0

Khairoutdinov, M., & Emanuel, K. A. (2010). Aggregated convection and the regulation of tropical climate. In *paper presented at the 29th Conference on Hurricanes and Tropical Meteorology* (p. 2.69). Tucson, AZ. Retrieved from https://ams.confex.com/ams/29Hurricanes/techprogram/paper_168418.htm

Mauritsen, T., & Stevens, B. (2015). Missing IRIS effect as a possible cause of muted hydrological change and high climate sensitivity in models. *Nature Geoscience*, *8*(5), 346–351. https://doi.org/10.1038/ngeo2414

Medeiros, B., Stevens, B., Held, I. M., Zhao, M., Williamson, D. L., Olson, J. G., & Bretherton, C. S. (2008). Aquaplanets, climate sensitivity, and low clouds. *Journal of Climate*, *21*(19), 4974–4991. https://doi.org/10.1175/2008JCLI1995.1

Morcrette, J.-J. (1991). Radiation and cloud radiative properties in the European Centre for Medium Range Weather Forecasts forecasting system. *Journal of Geophysical Research*, *96*(D5), 9121. https://doi.org/10.1029/89JD01597

Pierrehumbert, R. T. (1995). Thermostats, radiator fins, and the local runaway greenhouse. *Journal of Atmospheric Sciences*, *52*, 1784–1806. https://doi.org/10.1175/1520-0469(1995)052<1784:TRFATL>2.0.CO;2

Ringer, M. A., Andrews, T., & Webb, M. J. (2014). Global-mean radiative feedbacks and forcing in atmosphere-only and coupled atmosphere-ocean climate change experiments. *Geophysical Research Letters*, *5*, 4035–4042. https://doi.org/10.1002/2014GL060347

Senior, C. A., & Mitchell, J. F. B. (2000). The time-dependence of climate sensitivity. *Geophysical Research Letters*, *27*(17), 2685–2688. https://doi.org/10.1029/2000GL011373

Stevens, B., Sherwood, S. C., Bony, S., & Webb, M. J. (2016). Prospects for narrowing bounds on Earth's equilibrium climate sensitivity. *Earth's Future*, *4*, 512–522. https://doi.org/10.1002/2016EF000376

Vial, J., Dufresne, J. L., & Bony, S. (2013). On the interpretation of inter-model spread in CMIP5 climate sensitivity estimates. *Climate Dynamics*, *41*(11-12), 3339–3362. https://doi.org/10.1007/s00382-013-1725-9

Wing, A. A., Emanuel, K. A., Holloway, C. E., & Muller, C. (2017). Convective self-aggregation in numerical simulations: A review. *Surveys in Geophysics*, *38*, 1173–1197. https://doi.org/10.1007/s10712-017-9408-4

Zhou, C., Zelinka, M. D., & Klein, S. A. (2016). Impact of decadal cloud variations on the Earth's energy budget. *Nature Geoscience*, *9*, 871–874. https://doi.org/10.1038/NGEO2828